Eur Biophys J (2008) 37:627–638
DOI 10.1007/s00249-008-0286-z

ORIGINAL PAPER

Analysis of membrane-localized binding kinetics with FRAP

Omer Dushek · Raibatak Das · Daniel Coombs

Received: 24 October 2007 / Revised: 25 January 2008 / Accepted: 31 January 2008 / Published online: 26 February 2008

Abstract Interactions between plasma membrane-associated proteins on interacting cells are critical for many important biological processes. Few experimental techniques, however, can accurately determine the association and the dissociation rates between such interacting pairs when the two molecules diffuse on apposing membranes or lipid bilayers. In this study, we give a theoretical description of how and when fluorescence recovery after photobleaching (FRAP) experiments can be used to quantify these reaction rates. We analyze the effect of binding on FRAP recovery curves with a reaction–diffusion model and systematically identify different regimes in the parameter space of the association and the dissociation constants for which the full model simplifies into equivalent one-parameter models. Based on this analysis, we propose an experimental protocol that may be used to identify the kinetic parameters of binding in the appropriate parameter regime. We present simulated experiments illustrating our protocol and lay down guidelines for parameter estimation.

Keywords Fluorescence recovery after photobleaching · Surface binding kinetics · Mathematical model · Ligand–receptor binding · FRAP

Advanced neutron scattering and complementary techniques to study biological systems. Contributions from the meetings, "Neutrons in Biology", STFC Rutherford Appleton Laboratory, Didcot, UK, 11–13 July and "Proteins At Work 2007", Perugia, Italy, 28–30 May 2007.

Electronic supplementary material The online version of this article (doi:10.1007/s00249-008-0286-z) contains supplementary material, which is available to authorized users.

O. Dushek · R. Das · D. Coombs
Department of Mathematics, University of British Columbia, Vancouver, BC V6T 1Z2, Canada

O. Dushek · D. Coombs (✉)
Institute of Applied Mathematics, University of British Columbia, Vancouver, BC V6T 1Z2, Canada
e-mail: coombs@math.ubc.ca

R. Das
Department of Microbiology and Immunology, University of British Columbia, Vancouver, BC V6T 1Z2, Canada

Introduction

Many interfacial biological phenomena consist of interactions between molecules that are confined to two apposing membranes, often at the site of a cell–cell contact. A familiar example is the formation of an immune synapse between a T cell and an antigen presenting cell (APC), driven by interactions between T-cell receptor (TCR) and peptide–MHC (pMHC) complexes, and a host of coreceptors and adhesion molecules. Immune synapse formation can also be induced by substrate immobilized lipid bilayers containing a cognate pMHC and the adhesion molecule ICAM-1 (Grakoui et al. 1999). Substrate-immobilized lipid bilayers containing a cognate ligand have also been used to study stimulated activation of mast cells through the IgE-receptor complex (Wu et al. 2004). In order to properly understand these phenomena, in immunology and elsewhere, we require good experimental estimates of kinetic binding parameters for the ligand–receptor interaction. For instance, T-cell activation has been shown to depend on TCR-pMHC binding kinetics (reviewed in Coombs and Goldstein 2005).

Measurement of kinetic parameters for ligand–receptor binding can, for example, be performed using a Biacore optical sensor (Biacore, AB, Uppsala, Sweden). The receptor of interest is immobilized on the surface of a chip, and ligands

flow through a cell above the chip leading to changes in its optical properties (Garland 1996; Rich and Myszka 2000). It is then possible to estimate the on- and off-rates of the ligand–receptor interaction. However, a limitation of Biacore, and indeed of most conventional techniques for estimating binding kinetics, is that one or both binding partners are freely diffusing in a three- dimensional volume, whereas in a cell–cell or a cell–bilayer localized interaction they are restricted to diffuse on two-dimensional (2D) surfaces. Thus, Biacore measurements give three-dimensional (3D) reaction rates, that depend on the the molar concentration in solution, rather than 2D rates that depend on the surface densities of the the binding partners. Moreover, the receptor is immobilized on the chip surface and therefore, the potentially important influence of the plasma membrane is neglected.

A few alternative approaches have been used, with varying degrees of success, to estimate 2D binding affinities and reaction rates. Using quantitative fluorescence microscopy, the 2D affinity of the T-cell surface adhesion molecules, CD2 and CD28 to their ligands has been determined (Bromley et al. 2001; Dustin et al. 1996, 1997; Zhu et al. 2007) as well as the 2D affinity of certain TCR/pMHC interactions (Grakoui et al. 1999). Fluorescence resonance energy transfer (FRET) is another fluorescence microscopy technique that can be used to observe the association between two fluorophores (Selvin 2000). Because of its exquisite sensitivity to the distance between two fluorophores, FRET is ideal for measuring nanometer scale changes in spatial separation. FRET measurements have been primarily used for assaying qualitative changes in the association between interacting proteins (Hoffmann et al. 2005; Zal and Gascoigne 2004). Another possibility for quantifying binding interactions is to use dual color fluorescence correlation spectroscopy (FCS) which measures correlated fluctuations in the signals from two different fluorophores to infer a binding interaction between them (Kim and Schwille 2003; Kohl et al. 2005). Both FRET and FCS measurements are, at the present time, technically challenging to implement. Moreover, these techniques require distinct fluorescent tags on both the binding partners of an interacting pair. These difficulties may explain why there are very few measurements of kinetic parameters for membrane-bound protein interactions.

In this study, we focus on the technique of fluorescence recovery after photobleaching (FRAP), most commonly used to measure diffusion coefficients of biomolecules (Axelrod et al. 1976; Schlessinger et al. 1976), reviewed in (Rabut and Ellenberg 2004). FRAP has recently been used to measure kinetic parameters of 3D binding interactions between a fluorescently labeled ligand and its unlabeled binding partner (Beaudouin et al. 2006; Braga et al. 2007; Carrero et al. 2003; Hinow et al. 2006; Sprague et al. 2004), comprehensively reviewed in (Sprague and McNally 2005). These studies show that FRAP can yield 3D kinetic parameters in a variety of settings, but subject to certain assumptions that will not apply in the case of membrane-restricted binding interactions. For instance, (Carrero et al. 2003; Hinow et al. 2006; Sprague et al. 2004) assumed simple geometries and immobile binding sites for the labeled receptor. More recently, Braga et al. extended this analysis to the case when the binding sites are also mobile and applied their analysis to examine the diffusion of mRNA in the the nucleus (Braga et al. 2007). A potential limitation of all these studies, discussed further in (Pando et al. 2006), is that they yield compound parameters such as the true equilibrium constant multiplied by the free receptor concentration. Because the receptor is commonly assumed to be in excess in these studies, some care is required in interpreting the compound parameters obtained.

Here, we present an experimental protocol that can be utilized to measure true (not compound) kinetic parameters for a binding interaction between two mobile proteins diffusing on nearby membranes. We allow for diffusion of both the labeled receptor and the unlabeled ligand, and perform our analysis using the rectangular geometry that is commonly used in cell-surface experiments with a laser confocal scanning microscope. We systematically identify regions of parameter space in which the kinetic parameters can (theoretically) be measured as well as those in which they cannot. Finally, we fit a set of simulated FRAP recovery curves using the outlined protocol, and we provide guidelines for fitting experimental FRAP recovery curves to infer kinetic binding parameters.

Modeling

Full model

We begin our analysis with a reaction–diffusion system that governs the dynamics of two diffusing species on a 2D surface which bind with a 2D association rate k_{on}, and unbind at a rate k_{off}. One of the two species, the receptor, is labeled with a fluorophore, and it binds to a complementary ligand that is unlabeled. After photobleaching there is a subpopulation of unlabeled receptors and unlabeled receptor–ligand complexes. We use the following notation to describe the surface densities of all the relevant species:

$$\begin{aligned} f &= [\text{labeled receptor}],\\ f' &= [\text{unlabeled (photobleached) receptor}],\\ c &= [\text{labeled complex}],\\ c' &= [\text{unlabeled (photobleached) complex}],\\ s &= [\text{unlabeled ligand}], \end{aligned} \tag{1}$$

These quantities evolve according to the PDE system

$$\partial f/\partial t = D_f \nabla^2 f - k_{on} f s + k_{off} c, \quad (2a)$$

$$\partial c/\partial t = D_c \nabla^2 c + k_{on} f s - k_{off} c, \quad (2b)$$

$$\partial f'/\partial t = D_f \nabla^2 f' - k_{on} f' s + k_{off} c', \quad (2c)$$

$$\partial c'/\partial t = D_c \nabla^2 c' + k_{on} f' s - k_{off} c', \quad (2d)$$

$$\partial s/\partial t = D_s \nabla^2 s - k_{on} f' s + k_{off} c' - k_{on} f s + k_{off} c, \quad (2e)$$

where D_f, D_s, and D_c are diffusion coefficients of the free receptors, free ligands and bound complexes, respectively. We assume that the system is at chemical equilibrium prior to the FRAP experiment and that the fluorophores in the bleaching region are instantaneously photobleached at time $t = 0$. Thus, for $t < 0$, we have $f(t) = F_{eq}$, $f'(t) = 0$, $c(t) = C_{eq}$, $c'(t) = 0$, and $s(t) = S_{eq}$ where the subscript 'eq' indicates the equilibrium density of the three species. The photobleaching event at $t = 0$ creates a new subpopulation of unlabeled receptors and unlabeled complexes in a localized region, i.e. $f'(t) > 0$ and $c'(t) > 0$ for $t > 0$. Moreover, because photobleaching only removes the label and does not disturb the chemical equilibrium, we can assume that $s(t) = S_{eq}$ for all t. Therefore, we define a pseudo on-rate $k^*_{on} = k_{on} S_{eq}$, and rewrite Eqs. 2a and 2b as:

$$\partial f/\partial t = D_f \nabla^2 f - k^*_{on} f + k_{off} c, \quad (3)$$

$$\partial c/\partial t = D_c \nabla^2 c + k^*_{on} f - k_{off} c. \quad (4)$$

To obtain theoretical FRAP recovery curves we must solve Eqs. 7 and 8 with appropriate initial and boundary conditions reflecting the experimental geometry, and integrate the total fluorescence $f + c$ over the recovery region. The resulting quantity, $G_{fm}(t)$, gives the idealized FRAP recovery curve and is a function of the bleaching geometry, diffusion coefficients, and reaction rates. In Appendix A, we describe how to efficiently evaluate G_{fm}.

Note that because $s(t)$ is invariant in time, the dynamics of the labeled species are decoupled from those of the unlabeled species, resulting in a simpler system of equations to analyze. With these assumptions, Eqs. 7 and 8 govern the dynamics of the two labeled species and by solving them we obtain expressions for the observed fluorescence recovery (Appendix A). As illustrated in Fig. 1, we assume a rectangular bleaching region of dimensions X_b and Y_b along the x and y directions, respectively, and a monitoring region of dimensions X_m by Y_m that is a smaller subset of this bleaching region.

Reduced models

The full model defined by Eqs. 3 and 4 can be well-approximated by four simpler models in certain situations. These model reductions are briefly described below, and formally derived in the Supplementary Material. In each of these reduced models (1–4 below), the spatio-temporal dynamics are governed by simple diffusion equations of the form

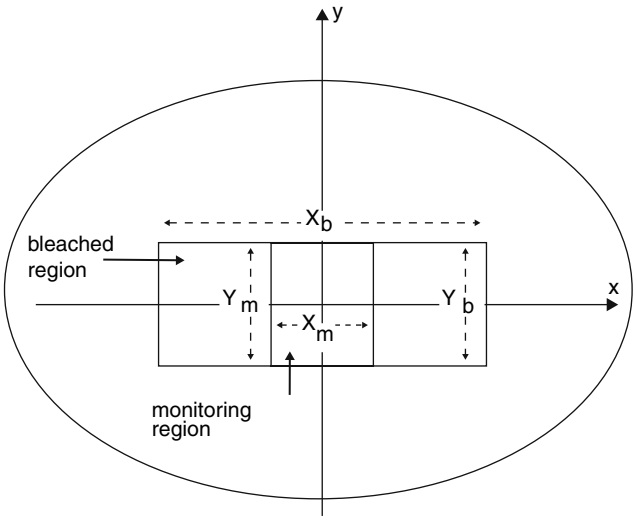

Fig. 1 The geometry of a typical confocal FRAP experiment

$$\partial u/\partial t = D \nabla^2 u \quad (5)$$

where D is a relevant diffusion coefficient for that model. The problem of fitting FRAP data to estimate D can then be solved as usual for the experimental geometry that is used (Axelrod et al. 1976; Dushek and Coombs 2007; Ellenberg et al. 1997; Goodwin and Kenworthy 2005). The solution for the the geometry shown in Fig. 1 is described in Appendix A.

Weighted diffusion (1)

One limit arises when k^*_{on} and k_{off} are not well-separated, but the lifetimes of the free and bound states are much smaller than their characteristic diffusive timescales. In this regime, the labeled receptor switches rapidly between its unbound form, with diffusion coefficient D_f, and its bound form with diffusion coefficient D_c. The FRAP recovery curve $G_{wd}(t) = U(t,D_{wd})$ (Eq. 14) then depends only on the effective (or weighted) diffusion coefficient:

$$D_{wd} = \frac{1}{1+K^*} D_f + \frac{K^*}{1+K^*} D_c \quad (6)$$

where $K^* = k^*_{on}/k_{off}$. In this regime, only D_{wd} can be determined from the data.

Independent diffusion (2)

When the diffusive timescales are much shorter than the lifetimes of the free and bound states, a labeled receptor remains in its (un)bound state on the timescale of the FRAP

experiment. In this case, there is no exchange between the pools of free and bound fluorophores, and FRAP recovery is a result of "independent diffusion" of these two pools with diffusion coefficients D_f and D_c, respectively. In this case, the FRAP recovery curve $G_{id}(t)$ is a simple weighted average of two independent FRAP recovery curves [$G_{pf}(t)$ for free receptors and $G_{pc}(t)$ for bound receptors]:

$$\frac{1}{1+K^*}G_{pf}(t) + \frac{K^*}{1+K^*}G_{pc}(t). \quad (7)$$

Receptor diffusion dominant (3)

When $k_{off} \gg k^*_{on}$, the bound complex rapidly dissociates, and the labeled receptor is almost always in the free state. The FRAP recovery curve $G_{pf}(t)$ is then a function of D_f alone. This regime is a subset of both the weighted and the independent diffusion regimes.

Complex diffusion dominant (4)

When $k^*_{on} \gg k_{off}$, the labeled receptor is almost always in the bound state. The FRAP recovery curve $G_{pc}(t)$ is then a function of D_c alone. Like the receptor diffusion dominant regime, this regime is a subset of both the weighted and the independent diffusion regimes.

The crucial difference between the full model and the reduced models is that, for the full model, but not any of the reduced models, all four parameters, D_f, D_c, k^*_{on} and k_{off} are required to completely describe the FRAP recovery curves. In contrast, in parameter regimes where the full model is reduced to one of these effective models, FRAP recovery curves are well-described by a smaller subset of parameters. Thus, in the weighted and independent diffusion regimes, the necessary parameters are D_f, D_c and K^*, and in the two diffusion dominant regimes, only D_f or D_c are sufficient to fully describe the FRAP recovery curves. Therefore in parameter regimes where one of these reduced models is applicable, one cannot, with any statistical confidence, estimate all four model parameters. Specifically, in the two diffusion dominant regimes no binding parameters can be estimated, and in the weighted and independent diffusion regimes, only the binding affinity K^* can be estimated. This categorization of the FRAP recovery curves is the basis of our proposed protocol described subsequently.

Structure of parameter space and model reductions

In the model reductions described earlier, we have made no assumptions about the relative magnitudes of D_f and D_c. If $D_f = D_c$ then we can see by adding Eqs. 7 and 8 that the full system reduces to a single diffusion equation and no binding information can be obtained. More generally, if D_f and D_c are close to each other, the region in parameter space where the full model applies is small. On the other hand, if the two diffusion coefficients are well separated then the analysis of Sprague et al. (2004) applies (see supplementary material).

We illustrate how the separation between D_f and D_c impacts the regions of parameter space where the model reductions are relevant in Fig. 2. We evaluate the sum of the squared residuals (SSR) between the full model and either the weighted or the independent diffusion reductions. In Fig. 2a–c we plot SSR contours as a function of k^*_{on} and k_{off} for biologically relevant values of D_f and D_c (Favier et al. 2001; Kenworthy et al. 2004). Further (Sprague et al. 2004), we consider the model reduction a good estimate to the FRAP recovery if SSR < 1. We note that the closer the two diffusion coefficients are to each other, the smaller is the region where only the two-parameter full model provides a better fit to the data (compare Fig. 2a, b). When the diffusion coefficients differ only by a factor of two, the region where only the two-parameter full model is accurate disappears (Fig. 2c). The structure of parameter space is also illustrated in Fig. 3d where all four regimes are shown (discussed later). As discussed in the following section, we utilize the existence of these different regions in the k^*_{on}–k_{off} parameter-space to quantify binding kinetics of the receptor–ligand interaction.

Proposed experimental protocol

In the previous section we identified four parameter regimes, in which the combined reaction–diffusion system (Eqs. 3, 4) is effectively reduced to a single diffusion equation (Eq. 5). As discussed earlier, in those parameter regimes, it is not possible to estimate the binding parameters k^*_{on} and k_{off} independently. To do so, we must first identify regions of parameter space where the full model fits the data, i.e. outside regimes 1–4. In this section, we propose an experimental protocol that, under suitable conditions, can be used to obtain these binding parameters by fitting a series of FRAP recovery curves. We consider an experimental system consisting of a cell bearing fluorescently labeled receptors on its surface, that is in contact with a suspended planar bilayer bearing unlabeled ligands at concentration S_T. We assume that the system is at chemical equilibrium before each experiment (achieved by waiting a sufficiently long time after the initial contact between the cell and the bilayer).

Measuring diffusion coefficients

The first step is to establish the diffusion coefficients D_f and D_c, if they are not already known. This can be done by

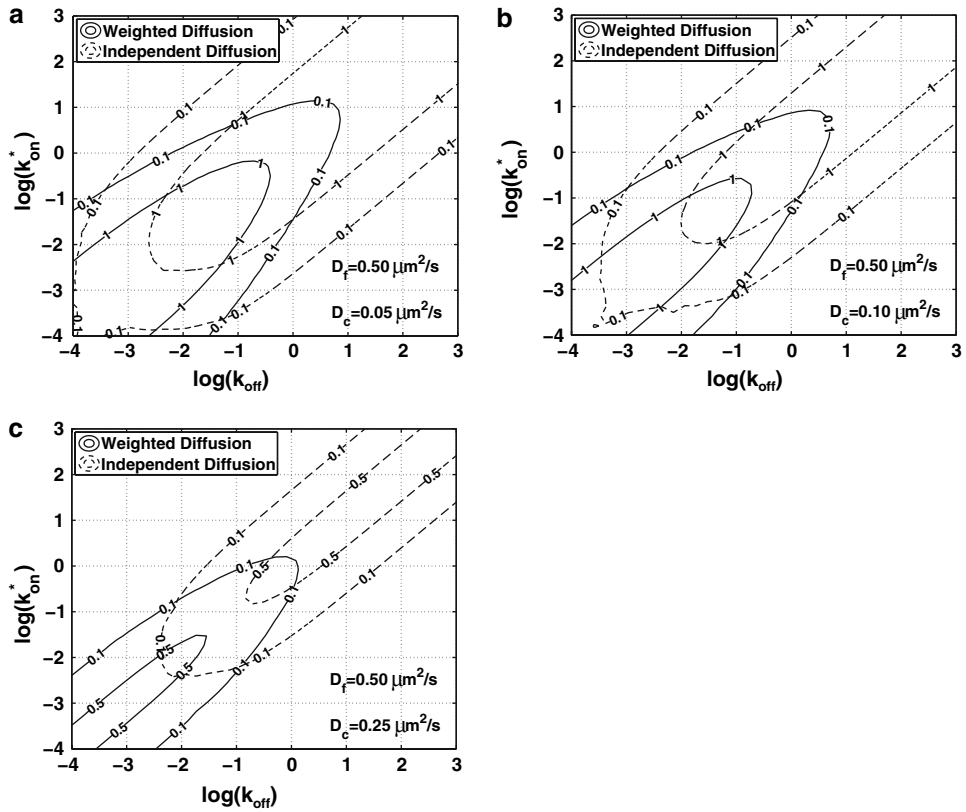

Fig. 2 Quantifying full model limits. We compute the sum of the squared residuals (SSR) between the full model, Eq. 21, and cases 1 and 2 for 200 equally spaced time points reaching 99% recovery. We plot SSR contours as a function of k^*_{on} and k_{off}. In **a**–**c** we see that the region where the full model is valid progressively decreases as D_c approaches D_f. Parameters: $X_b = Y_b = X_m = Y_m = 2$ μm

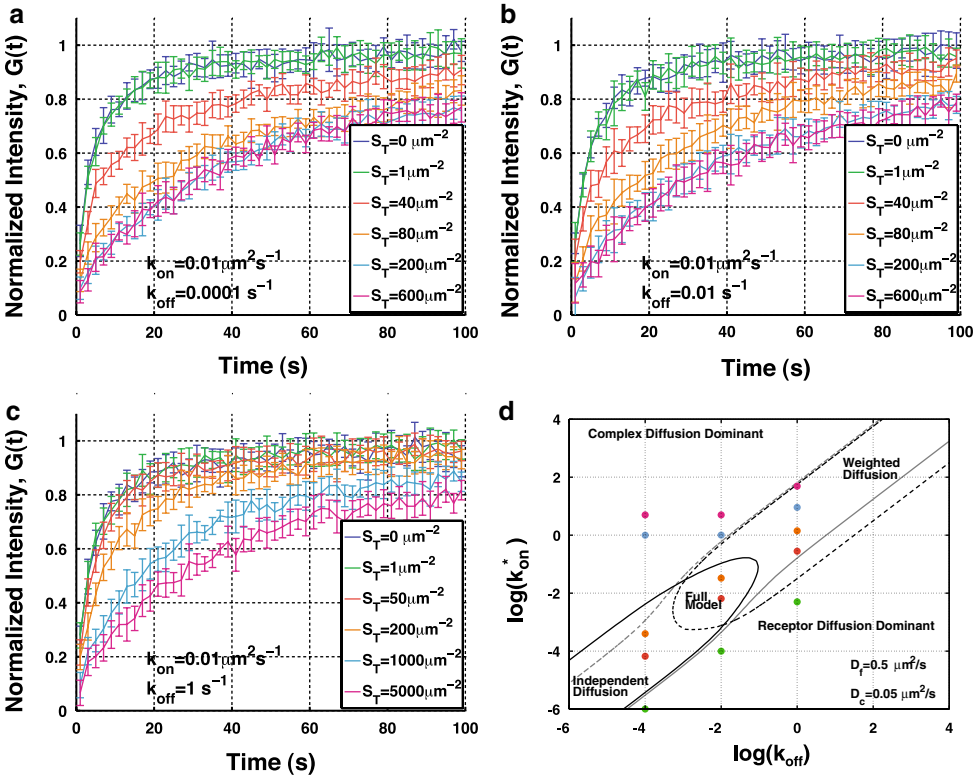

Fig. 3 Numerically simulated FRAP titration experiments demonstrate the effect of increasing ligand density on FRAP recovery dynamics. FRAP curves (**a**–**c**) were numerically simulated as described in the text, with parameter values listed in Table 1, and the total ligand density S_T indicated in the legend. The corresponding points on the k^*_{on}–k_{off} parameter space are shown in **d**, along with the contours indicating the applicable model regimes. Only contours of SSR = 1 are shown (*gray*: pure diffusion (free), *dotted gray*: pure diffusion (bound), *black*: weighted diffusion, *dotted black*: independent diffusion). The contour lines were generated as described in Fig. 2

performing a straightforward FRAP experiment in the absence of the ligand (i.e. $S_T = 0$), and fitting the recovery curve to Eq. 9 to establish D_f. The FRAP experiment can then be repeated with a saturating density of the ligand (such that all the receptors are engaged) to establish D_c. These two FRAP experiments correspond to the two pure-diffusion limits of the full model (cases 3 and 4), respectively. If D_f is found to be close to D_c then successful measurement of the binding kinetic parameters is not expected in our protocol.

Ligand titration experiment

Having established the diffusion coefficients of the free and bound forms, the key experiment is to 'titrate' the ligand density, by performing FRAP experiments with a range of intermediate ligand densities. As the total ligand density, S_T, increases, the equilibrium free ligand concentration, S_{eq}, also increases according to the following equation (derived from a conservation equation):

$$S_{eq} = \frac{K(S_T - F_T) - 1 + \sqrt{[1 + K(S_T + F_T)]^2 - 4S_T F_T}}{2K}, \tag{8}$$

where F_T is the total receptor concentration and $K = k_{on}/k_{off}$ is the 2D equilibrium constant. As a result, the pseudo-on rate, $k^*_{on} = k_{on}\, S_{eq}$, also increases, and the system traverses the k^*_{on}–k_{off} parameter-space parallel to the k^*_{on} axis (Fig. 3d). As shown in Fig. 3d, for different k^*_{on} values, a different model will best describe the FRAP recovery curve. In other words, as the total ligand concentration, S_T is varied in a controlled fashion, each resulting FRAP recovery curve is best fitted by a particular model, depending on the location of the system on the k^*_{on}–k_{off} phase plane.

In Fig. 3a–c the recovery dynamics are progressively slower as the ligand density increases because receptor–ligand binding effectively slows down the diffusion of the receptors, $D_c < D_f$. The idea is to perform a series of FRAP experiments traversing the k^*_{on}–k_{off} phase plane (Fig. 3d) and, for each experiment, establish which model best describes the FRAP recovery curve. For example, for the recovery curves shown in Fig. 3b, with $k_{off} = 0.01\ s^{-1}$, the system traverses from case 3 (receptor diffusion dominant), via the full model regime, to case 4 (complex diffusion dominant).

Data fitting

The goal is now to classify each of the recovery curves for intermediate ligand densities into one of case 1, case 2 or the full model. Each recovery curve is initially fit using all three different models: the two-parameter full model (Eq. 21), a one-parameter diffusion model (case 1: Eqs. 6, 14), and a one-parameter independent diffusion model (case 2: Eqs. 7, 14). For each fit, we determine the best-fit value of the parameter(s) for that model. The relative quality of the three fits are then compared on the basis of the sum-of-squared-residuals (SSR), where a lower SSR indicates a better fit. However, to compensate for the difference in number of parameters, we use Akaike's Information criterion (AIC) as a metric for comparing the quality of fits (Akaike 1973; Motulsky and Christopoulos 2004). AIC, defined as:

$$\mathrm{AIC} = n \ln(\mathrm{SSR}/n) + 2P \tag{9}$$

where n is the number of data points, and P is the number of parameters, balances the gain due to a lowered SSR with the penalty for an increase in the number of parameters. The model with the lowest AIC value is considered to be the best descriptor of the experimental data.

We use the quality of fits, as quantified by AIC (Eq. 9), to select the appropriate model(s) for parameter estimation. For each recovery curve, we identify the fit with the lowest AIC value. The other two fits are quantified by the difference in their AIC value from this fit. The difference, ΔAIC, is a measure of the probability of the other model being an equally likely descriptor for the FRAP recovery curves. The probability of each model is given by'

$$p = \frac{\exp(-\Delta\mathrm{AIC}/2)}{1 + \exp(-\Delta\mathrm{AIC}/2)}. \tag{10}$$

In practice, a fit with $\Delta\mathrm{AIC} \geq 10$ indicates that the model under consideration is extremely unlikely compared to the best model, and a fit with $\Delta\mathrm{AIC} \leq 2$ indicates that the model is nearly as likely as the best model (Motulsky and Christopoulos 2004).

We use the relative quality-of-fit for the three models to determine (for each one of the the FRAP experiments) whether or not k^*_{on}, k_{off} and K^* can be found. Three scenarios emerge:

Scenario 1. $\Delta\mathrm{AIC} < 10$ for both one-parameter models. The system is in a pure diffusion limit and no estimates of binding parameters can be obtained.

Scenario 2. $\Delta\mathrm{AIC} < 10$ for exactly one of the one-parameter models. The system is in the regime best described by that model, and the best-fit value of the pseudo-affinity K^* is obtained.

Scenario 3. $\Delta\mathrm{AIC} \geq 10$ for both the one-parameter models. The system is in the full model regime and best-fit values of k^*_{on} and k_{off} are obtained.

This procedure rejects any fits with $\Delta AIC \geq 10$ as being too unreliable for parameter estimation. Categorizing the fits into these three scenarios is motivated by the existence of different model regimes in the $k_{on}^{*}-k_{off}$ parameter space. As shown in Fig. 3d, the points corresponding to the recovery curves for a titration will transition from one diffusion-dominant regime to another diffusion-dominant regime as the ligand concentration is increased. In the diffusion-dominant regimes, the recovery dynamics are well-described by either of the two one-parameter models (scenario 1). For intermediate concentrations, however, the system is in either the full model regime, or in a one-parameter model regime. When the system is in a weighted-diffusion or independent-diffusion regime, the recovery dynamics are best fitted exclusively by the corresponding one-parameter model, and not the other one (scenario 2). Finally, in scenario 3, the system is in the full model regime, and neither of the two one-parameter reductions are appropriate descriptors of recovery dynamics.

Parameter estimation

In scenario 1, the system is in a regime where no binding information can be obtained. In scenario 2, we determine the pseudo-affinity K^{*} using the one-parameter model with $\Delta AIC < 10$. If this is the independent diffusion model, then the parameter K^{*} is directly determined from the fit. If this is the weighted diffusion model, then the fitted parameter is D_{wd}, and K^{*} is obtained by rearranging equation 6:

$$K^{*} = \frac{D_f - D_{wd}}{D_{wd} - D_f} \tag{11}$$

Additionally, in scenario 2, it is also possible that $\Delta AIC < 10$ for the full model, and we have another estimate for K^{*} from the full model fit, given by the ratio k_{on}^{*}/k_{off}. We combine the parameter estimates from the two fits by using the probability, P (Eq. 10), of each model as a weight, and calculate the weighted mean of the best-fit K^{*}. In scenario 3 fitting the full model provides estimates of k_{on}^{*} and k_{off}, as well as $K^{*} = k_{on}^{*}/k_{off}$.

Estimates of the pseudo-affinity, K^{*} (scenario 2) and the pseudo-association rate, k_{on}^{*} (scenario 3), can be converted to the true 2D affinity, $K = K^{*}/S_{eq}$ and association rate, $k_{on} = k_{on}^{*}/S_{eq}$ using the free ligand concentration S_{eq}, given by:

$$S_{eq} = S_T - \frac{K^{*}}{1 + K^{*}} F_T, \tag{12}$$

where S_T and F_T are the known total ligand and total receptor concentrations, respectively, and we use the best-fit estimate of K^{*} from the fits. However, the estimate of the true parameters is unreliable when $S_{eq} \approx 0$ because of the small value of the denominator in the expressions for k_{on} and K. In practice, we find that when the ratio S_{eq}/S_T becomes small, that is, at equilibrium only a negligible fraction of the total ligand is unbound, the estimates of the true parameters can deviate significantly from their actual value.

Simulated experiments

Simulated FRAP titrations

To test our protocol, we simulated three sets of numerical experiments, and applied in the earlier data-fitting and parameter-estimation procedure to the simulated datasets. These simulations model the interaction between a receptor–ligand pair, with a fixed k_{on} and three different k_{off} values, representing, for example, a range of binding affinities of pMHC for a particular TCR. Table 1 lists the parameter values used to generate the simulated data. We use biologically relevant reaction rates between cell surface proteins (Davis et al. 2003; Grakoui et al. 1999), typical diffusion coefficients for membrane proteins (Favier et al. 2001; Kenworthy et al. 2004), and commonly used sizes for the bleach and monitoring regions (Kenworthy et al. 2004). The Einstein–Stokes relation predicts that if two particles with individual diffusion coefficients D_f and D_s bind together, the complex will have diffusion coefficient $D_f D_s/(D_f + D_s)$ (assuming their drag coefficients are additive). Supposing $D_f \simeq D_s$ for similar surface proteins, this estimate yields that the complex will be roughly half as diffusive. However, proteins diffusing in a lipid membrane may not behave as ideal Brownian particles (Saffman and Delbruck 1975), and upon binding the resulting complex may have a drag coefficient different from the sum of the individual drag coefficients. We therefore take this

Table 1 Parameters used for numerically simulating FRAP recovery curves shown in Fig. 3

Parameter	Value
D_f	0.5 $(\mu m)^2 s^{-1}$
D_c	0.05 $(\mu m)^2 s^{-1}$
F_T	100 $(\mu m)^{-2}$
X_b	6 μm
Y_b	3 μm
X_m	2 μm
Y_m	3 μm
k_{on}	0.01 $(\mu m)^2 s-1$
k_{off}	10^{-4} s^{-1} (Experiment A, Fig. 3a)
	10^{-2} s^{-1} (Experiment B, Fig. 3b)
	1 s^{-1} (Experiment C, Fig. 3c)

estimate as only an upper bound on D_c, and assume D_c = 0.1 D_f in our simulations (Table 2).

For each experiment, we chose a set of increasing S_T values to simulate the effect of titrating in an increasing density of pMHC into the lipid bilayer. The corresponding recovery curves are shown in Figs. 3a–c. Individual recovery curves were generated using the full model (see Appendix A) for the given choice of parameter values. 10% Gaussian noise was added to the solution, to model typical experimental errors in FRAP measurements. Each FRAP recovery curve shown in Fig. 3a–c is the average of ten such individual recovery curves. The location of points on the k^*_{on}–k_{off} parameter-space are indicated by corresponding colored dots in Fig. 3d. The SSR contours in Fig. 3d indicate that for different S_T values (i.e. different k^*_{on} values through Eq. 8) a different model will best describe the FRAP recovery.

Fitting simulated data

We applied the fitting procedure previously described to the simulated FRAP titrations. For each experiment, we first fit the recovery curves with $S_T = 0$ to Eq. 9, and determined the best-fit values of D_f = [0.50,0.50,0.49] $(\mu m)^2 s^{-1}$, for experiments A–C (Fig. 3a–c), respectively. Similarly, for each experiment, we also fit the titrations with the highest S_T value and obtained the best-fit values of D_c = [0.050,0.051,0.059] $(\mu m)^2 s^{-1}$, respectively.

Having established the diffusion coefficient of the free receptor and bound complex, we next fit the intermediate

Table 2 Parameter values used in numerical simulations, and the estimates from fitting the simulated FRAP titration data

k_{off} s^{-1}	K $(\mu m)^{-2}$	S_T $(\mu m)^{-2}$	K^*	k^*_{on} s^{-1}	Fit scenario
Simulation parameters					
Experiment A					
0.0001	100	1	0.0101	1.01×10^{-6}	1
		40	0.666	6.66×10^{-5}	2
		80	3.99	3.99×10^{-4}	2
		200	1.00×10^{-4}	1.00	1
Experiment B					
0.01	1	1	0.0100	1.00×10^{-4}	1
		40	0.649	6.49×10^{-3}	3
		80	3.29	0.0329	3
		200	1.01×10^{-2}	1.01	1
Experiment C					
1	0.01	1	5.01×10^{-3}	5.01×10^{-3}	1
		50	0.281	0.281	2
		200	1.41	1.41	2
		1000	9.10	9.10	2

Experiment	S_T $(\mu m)^{-2}$	K^*	k^*_{on} s^{-1}	k_{off} s^{-1}	S_{eq}/S_T	K $(\mu m)^{-2}$	k_{on} $(\mu m)^2$ s^{-1}
Fitted parameters							
A	1						
	40	0.667			1.25×10^{-4}		
	80	3.88			0.00631		
	200						
B	1						
	40	0.692	7.67×10^{-3}	0.0111	−0.0222		
	80	3.31	0.0309	0.00933	0.0401	1.03	0.00963
	200						
C	1						
	40	0.269			0.576	0.00934	
	80	1.46			0.703	0.0104	
	200	11.082			0.908	0.0122	

FRAP recovery curves in each experiment to all the three models, i.e. weighted diffusion (case 1), independent diffusion (case 2), and the full model. We used the best-fit values of D_f and D_c, as determined from fitting the two limiting FRAP curves, as known constants in these equations. Thus, for each intermediate FRAP curve in a titration we obtained the best-fit value of the the model parameters D_{wd}, K^*, k^*_{on} and k_{off}. These best-fit parameter values, the SSR from the corresponding fits, and the resulting AIC statistics for the intermediate FRAP recovery curves from all three titrations are shown in the supplementary material.

Based on the ΔAIC values of the three fits for each curve, we identify the particular scenario that is applicable for parameter estimation. As described in detail previously, for a fit in scenario 2 we can determine the pseudo-affinity, K^*, and for a fit in scenario 3 we can also determine the pseudo-on rate k^*_{on} and the off-rate k_{off}. In Table 1 we list the identified fitting scenario for each FRAP curve, and parameter estimates for fits in scenarios 2 and 3. Comparing the fitted parameter values with those used for simulating the data, we note that for all fits under scenarios 2 and 3, the fitted parameter values are close to their actual values.

We also list the ratio S_{eq}/S_T in Table 1. This is determined using the known S_T, and F_T values, and the fitted K^* values. When this ratio $S_{eq}/S_T > 0.01$, we are additionally able to estimate the true 2D on rate k_{on} (Experiment B), and the true 2D affinity K^* (Experiments B and C) for the ligand–receptor pair. The ratio S_{eq}/S_T measures the fraction of ligands that are in an unbound state at equilibrium. Thus, this fraction is small for high-affinity ligands, and also at low-ligand densities. Thus, under these conditions, we are unlikely to reliably determine the true 2D kinetic parameters. In the previous numerical simulations, the receptor–ligand affinity is the greatest for Experiment A, for which we observe the smallest values of this ratio. For the lower affinities in Experiments B and C, S_{eq}/S_T is large enough for progressively higher ligand concentrations, allowing reliable estimates of the true 2D parameters.

Experimental outlook

In the previous sections we proposed a confocal FRAP-based protocol to measure true 2D binding parameters between a membrane-associated receptor–ligand pair, and tested its applicability with numerically simulated FRAP recovery curves. Here, we point out some experimental challenges that need to be overcome for a successful application of this protocol.

A key requirement of our protocol is the prior knowledge of the diffusion coefficients of free and bound forms of the receptor. We suggest conducting FRAP experiments in the absence of any ligand to establish the former, and in the presence of a saturating concentration of the ligand, to establish the latter. A limitation of this approach may be the low surface density of free receptors resulting in a low signal to noise ratio in the FRAP experiments. Nonetheless, translational diffusion coefficients of a variety of cell-surface proteins, including a GFP conjugated TCR, have been successfully measured using FRAP (Favier et al. 2001; Kenworthy et al. 2004), and we expect that for an experimental system of interest such measurements will be feasible. Alternatively, overexpressing the receptor of interest could further enhance the signal to noise ratio for receptors with low surface density. When the receptors are engaged, possible complications in FRAP measurement may arise from clustering of receptors into microclusters, observed for TCR–pMHC interactions (Campi et al. 2005) or a substantial immobile fraction (Favier et al. 2001). However, these effects are cytoskeleton-dependent, and are abrogated in the presence of pharmacological inhibitors of actin polymerization such as latranculin-A.

The more challenging requirement of our protocol is the accurate and reproducible measurement of the surface densities of both binding partners. In cells expressing a genetically encoded fluorescently-labeled protein, one often observes a heterogenous population with varying expression levels, that may be difficult to quantify, without a detailed knowledge of the photophysical properties of the fluorophore in an intracellular environment. Fluorescent calibration beads have been successfully used to quantify the surface density of TCR on cells in similar experiments (Campi et al. 2005). Further, it is possible to maintain a relatively uniform expression level by isolating a single clone and proliferating it, or alternatively by sorting cells on the basis of fluorescence intensity and retaining a population with a relatively homogenous expression level. Likewise, by loading liposomes with varying concentrations of the specific ligand during bilayer preparation, it is possible to control the ligand surface density on a lipid bilayer (Grakoui et al. 1999; Varma et al. 2006; Zhu et al. 2007).

Lastly, as with all FRAP experiments care must be taken to minimize errors due to the finite bleach time (Braga et al. 2004; Klonis et al. 2002), the shape of the bleaching beam (Braga et al. 2004) and the finite domain (Dushek and Coombs 2007). Incomplete FRAP recovery, in the absence of binding, could arise from an immobile fraction (Klonis et al. 2002). By defining M_f to be the fraction of proteins that are mobile, we can correct for situation when $M_f < 1$ by simply multiplying the FRAP recovery by this fraction (see Klonis et al. 2002; Dushek and Coombs 2007). Additionally, our method and indeed the most common FRAP analyses are not applicable when there is appreciable membrane curvature. For a detailed discussion

of the applicability of FRAP to curved membranes see Sbalzarini et al. (2006).

Conclusions

We have outlined an experimental protocol for determination of kinetic parameters for membrane-restricted binding of a ligand and receptor, based on titrating the density of the unlabeled substrate (ligand) and measuring FRAP recovery dynamics of the labeled receptor. As the ligand density increases, the system transitions from a diffusion-dominant regime where the protein is predominantly unbound, to another diffusion-dominant regime where the protein is predominantly bound. The passage between these two diffusion dominant regimes is through an intermediate regime where either the full model, or one of either the weighted-diffusion model, or the independent diffusion model are applicable.

As described earlier, and illustrated in Fig. 2, the extent of this intermediate regime in parameter space is determined by the separation between the diffusion coefficients of the free and the bound forms of the fluorophore. Thus, when the diffusion coefficients of the bound and free forms of a protein are sufficiently different, this method allows for an estimation of the true two-dimensional on and off rates for the binding or the true two-dimensional affinity. Alternatively, if the diffusion coefficients are not sufficiently different, this technique cannot discern any kinetic information. Due to this constraint, it may be necessary to slow down the diffusion of the ligand (and therefore, presumably of the bound complex), for instance via adhesion to a large, or a slowly diffusing particle.

A distinct advantage of our technique is the need to fluorescently label only one of the binding partners. Further, the feasibility of our approach is at least partially evident from a number of recent studies where FRAP has been used to measure 3D binding constants in a variety of settings (e.g. Braga et al. 2007; Carrero et al. 2003; Hinow et al. 2006; Sprague et al. 2004). The study of Sprague et al. assumed that the unlabeled binding partner was immobile, whereas we analyze a more general model without this constraint. Further, for sufficiently different diffusion coefficients, our method allows us to fit for the 2D rate constant k_{on} rather than the compound rate $k^*_{on} = k_{on}S_{eq}$. We additionally specialize to the commonly used geometry of confocal FRAP on cell surfaces. Our method also represents an alternative to that of Braga et al. (2007), where FRAP measurements were used to elucidate the binding-mediated diffusion of mRNA fragments in the nucleus of HeLa cells. In that study, a relatively complex method was used to fit the data, involving repeated numerical solution of the partial differential equations for the diffusing species. Our fitting technique is conceptually simpler, involving fitting only a relatively simple expression to the data.

We also point out some experimental challenges for a successful implementation of our protocol. One of the key requirement of our method is an accurate estimation of the surface density of the two binding partners, and we foresee this to be a key experimental challenge toward a successful implementation. Our analysis has also ignored other sources of experimental error such as background photobleaching of the fluorophore, fluorescence recovery during the finite bleaching time, geometric effects stemming from the beam shape, etc. discussed elsewhere (Rabut and Ellenberg 2004). Notwithstanding these difficulties, our proposed experimental technique offers a conceptually simple alternative to existing methods for quantifying receptor–ligand binding interactions on membranes.

Acknowledgments This work was supported by NSERC and MITACS NCE. We are indebted to Salvatore Valitutti for helpful discussions.

Appendix: evaluation of theoretical FRAP recovery curves

Simple FRAP analysis

In typical surface photobleaching experiments, the photobleached area is much smaller than the total area of the plasma membrane. Therefore, we can assume that the domain is effectively infinite in extent without introducing appreciable error. For the parameter regimes that reduce to simple diffusion (cases 1–3), the FRAP recovery curve is determined by Eq. 9 with initial conditions

$$u(t=0) = 1 - [H(x+X_b/2) - H(x-X_b/2)][H(y+Y_b/2) - H(y-Y_b/2)] \quad (13)$$

where $H(x)$ is the Heaviside step-function. This is easily solved by Fourier transform, and the desired FRAP recovery curve is then obtained by integrating u over the monitoring region $(-X_m/2 \le x \le X_m/2, -Y_m/2 \le y \le Y_m/2)$, to obtain the following expression for the theoretical FRAP recovery curve (Dushek and Coombs 2007):

$$\begin{aligned} U(t,D) = 1 - \frac{\sqrt{Dt}}{2\pi X_m Y_m} &\left\{\sqrt{\pi}[X_+\mathrm{erf}(X_+) - X_-\mathrm{erf}(X_-)] \right. \\ &\left. + \left[\exp(-X_+^2) - \exp(-X_-^2)\right]\right\} \\ &\times \left\{\sqrt{\pi}[Y_+\mathrm{erf}(Y_+) - Y_-\mathrm{erf}(Y_-)] \right. \\ &\left. + \left[\exp(-Y_+^2) - \exp(-Y_-^2)\right]\right\} \end{aligned} \quad (14)$$

where we define

$$X_{\pm} = \frac{X_b \pm X_m}{4\sqrt{Dt}} \quad \text{and} \quad Y_{\pm} = \frac{Y_b \pm Y_m}{4\sqrt{Dt}}. \tag{15}$$

This expression can be fit to data to determine the parameter D.

FRAP with binding kinetics

We are now concerned with solving Eqs. 3 and 4. Taking the Fourier transform (denoted with hats), we obtain the linear system

$$\partial\hat{f}/\partial t = D_{\mathrm{f}}(-4\pi^2 q_x^2 - 4\pi^2 q_y^2)\hat{f} - k_{\mathrm{on}}^{*}\hat{f} + k_{\mathrm{off}}\hat{c}, \tag{16a}$$

$$\partial\hat{c}/\partial t = D_{\mathrm{c}}(-4\pi^2 q_x^2 - 4\pi^2 q_y^2)\hat{c} + k_{\mathrm{on}}^{*}\hat{f} - k_{\mathrm{off}}\hat{c}. \tag{16b}$$

We define $q_f = 4\pi^2 D_{\mathrm{f}}\,(q^2{}_x + q^2{}_y) + k_{\mathrm{on}}^{*}$ and $q_c = 4\pi^2\, D_{\mathrm{c}}\,(q^2{}_x + q^2{}_y) + k_{\mathrm{off}}$ to obtain

$$\frac{\partial\hat{f}}{\partial t} = -q_f\hat{f} + k_{\mathrm{off}}\hat{c}, \tag{17a}$$

$$\frac{\partial\hat{c}}{\partial t} = k_{\mathrm{on}}^{*}\hat{f} - q_c\hat{c}, \tag{17b}$$

whose solutions are

$$\begin{aligned}\hat{f} = \frac{1}{v}\big[&(1/2)\hat{f}(t=0)\big(\exp(D_1 t)(q_c - q_f + v)\\ &+\exp(D_2 t)(-q_c + q_p + v)\big)\\ &+k_{\mathrm{off}}\hat{c}(t=0)(\exp(D_1 t) - \exp(D_2 t))\big],\end{aligned} \tag{18a}$$

$$\begin{aligned}\hat{c} = \frac{1}{v}\big[&(1/2)\hat{c}(t=0)\big(\exp(D_1 t)(-q_c + q_f + v)\\ &+\exp(D_2 t)(q_c - q_f + v)\big)\\ &+k_{\mathrm{on}}^{*}\hat{f}(t=0)(\exp(D_1 t) - \exp(D_2 t))\big]\end{aligned} \tag{18b}$$

where $v = [(q_c - q_f)^2 + 4k_{\mathrm{on}}^{*}\,k_{\mathrm{off}}]^{1/2}$, $D_1 = (-q_c - q_f + v)/2$, $D_2 = (-q_c - q_f - v)/2$. $\hat{f}(t=0)$ and $\hat{c}(t=0)$ are Fourier transforms of the initial conditions,

$$\hat{f}(t=0) = -F_{\mathrm{eq}}\mathrm{sinc}(\pi X_b q_x)\mathrm{sinc}(\pi Y_b q_y) + F_{\mathrm{eq}}\delta(q_x)\delta(q_y) \tag{19a}$$

$$\hat{c}(t=0) = -C_{\mathrm{eq}}\mathrm{sinc}(\pi X_b q_x)\mathrm{sinc}(\pi Y_b q_y) + C_{\mathrm{eq}}\delta(q_x)\delta(q_y). \tag{19b}$$

where $F_{\mathrm{eq}} = k_{\mathrm{off}}/(k_{\mathrm{on}}^{*} + k_{\mathrm{off}})$ and $F_{\mathrm{eq}} = k_{\mathrm{on}}^{*}/(k_{\mathrm{on}}^{*} + k_{\mathrm{off}})$. We obtain these relationships by assuming that the system is in equilibrium prior to the FRAP experiment ($k_{\mathrm{on}}^{*}\,F_{\mathrm{eq}} = k_{\mathrm{off}}\,C_{\mathrm{eq}}$) and the FRAP recovery can be normalized to unity ($F_{\mathrm{eq}} + C_{\mathrm{eq}} = 1$), see Sprague et al. (2004).

It is not possible to obtain an analytical inverse Fourier transform of these equations, and therefore theoretical FRAP recovery curves must be numerically computed. These are obtained by integrating the sum $f + c$ over the monitoring region, and dividing by the area of the monitoring region to obtain the mean fluorescence intensity over this area. Thus, for a rectangular monitoring region of dimensions X_m ($\leq X_b$) by Y_m ($\leq Y_b$), the recovery curve is given by

$$G_{\mathrm{fm}}(t) = \left(\int_{-X_m/2}^{X_m/2}\mathrm{d}x\int_{-Y_m/2}^{Y_m/2}\mathrm{d}y[f(t,x,y) + c(t,x,y)]\right)/(X_m Y_m), \tag{20}$$

and, by definition of the inverse Fourier transform,

$$\begin{aligned}G_{\mathrm{fm}}(t) &= \frac{1}{4X_m Y_m}\int_{-X_m}^{X_m}\mathrm{d}x\int_{-Y_m}^{Y_m}\mathrm{d}y\int_{-\infty}^{\infty}\mathrm{d}q_x\int_{-\infty}^{\infty}\mathrm{d}q_y\big[\hat{f}(t,q_x,q_y)\\ &\quad+\hat{c}(t,q_x,q_y)\big]\times\exp(2\pi\imath q_x x)\exp(2\pi\imath q_y y)\\ &= \int_{-\infty}^{\infty}\mathrm{d}q_x\int_{-\infty}^{\infty}\mathrm{d}q_y\big[\hat{f}(t,q_x,q_y) + \hat{c}(t,q_x,q_y)\big]\\ &\quad\mathrm{sinc}(\pi q_x X_m)\mathrm{sinc}(\pi q_y Y_m)\\ &= 4\int_{0}^{\infty}\mathrm{d}q_x\int_{0}^{\infty}\mathrm{d}q_y\big[\hat{f}(t,q_x,q_y) + \hat{c}(t,q_x,q_y)\big]\\ &\quad\mathrm{sinc}(\pi q_x X_m)\mathrm{sinc}(\pi q_y Y_m),\end{aligned} \tag{21}$$

which we compute by numerical integration. We found integrating to 15–20 in q_x and q_y yields sufficient accuracy for our purposes. Using the Matlab function `quadl`, the above integral can be evaluated 100 times (typical number of images in FRAP experiments) in approximately 3 s, allowing parameter fits in a reasonable timeframe using a standard fitting procedure. All fits presented in this work were carried out using the Matlab function `lsqcurvefit`.

References

Akaike H (1973) Information theory as an extension of the maximum likelihood principle. In: Petrov B, Csaki F (eds) 2nd international symposium on information theory. Akademiai Kiado, Budapest, pp 267–281

Axelrod D et al (1976) Mobility measurement by analysis of fluorescence photobleaching recovery kinetics. Biophys J 16:1055–1069

Beaudouin J et al (2006) Dissecting the contribution of diffusion and interactions to the mobility of nuclear proteins. Biophys J 90(6):1878–1894

Braga J et al (2004) Intracellular macromolecular mobility measured by fluorescence recovery after photobleaching with confocal laser scanning microscopes. Mol Biol Cell 15(10):4749–4760

Braga J et al (2007) A reaction-diffusion model to study RNA motion by quantitative fluorescence recovery after photobleaching. Biophys J 92(8):2694–2703

Bromley SK et al (2001) The immunological synapse and CD28–CD80 interactions. Nat Immunol 2(12):1159–1166

Campi G et al (2005) Actin and agonist MHC–peptide complex-dependent T cell receptor microclusters as scaffolds for signaling. J Exp Med 202(8):1031–1036

Carrero G et al (2003) Using FRAP and mathematical modeling to determine the in vivo kinetics of nuclear proteins. Methods 29(1):14–28

Coombs D, Goldstein B (2005) T cell activation: kinetic proofreading, serial engagement and cell adhesion. J Comput Appl Math 184:121–139

Davis MM et al (2003) Dynamics of cell surface molecules during T cell recognition. Annu Rev Biochem 72:717–742

Dushek O, Coombs D (2007) Improving parameter estimation for cell surface FRAP data. J Biochem Biophys Methods. doi: 10.1016/j.jbbm.2007.07.002

Dustin ML et al (1996) Visualization of CD2 interaction with LFA-3 and determination of the two-dimensional dissociation constant for adhesion receptors in a contact area. J Cell Biol 132(3):465–474

Dustin ML et al (1997) Low affinity interaction of human or rat T cell adhesion molecule CD2 with its ligand aligns adhering membranes to achieve high physiological affinity. J Biol Chem 272(49):30889–30898

Ellenberg J et al (1997) Nuclear membrane dynamics and reassembly in living cells: targeting of an inner nuclear membrane protein in interphase and mitosis. J Cell Biol 138:1193–1206

Favier B et al (2001) TCR dynamics on the surface of living T cells. Int Immunol 13(12):1525–1532

Garland PB (1996) Optical evanescent wave methods for the study of biomolecular interactions. Q Rev Biophys 29:91–117

Goodwin JS, Kenworthy A (2005) Photobleaching approaches to investigate diffusional mobility and trafficking of Ras in living cells. Methods 37:154–164

Grakoui A et al (1999) The immunological synapse: a molecular machine controlling T cell activation. Science 285:221–227

Hinow P et al (2006) The DNA binding activity of p53 displays reaction-diffusion kinetics. Biophys J 91:330–342

Hoffmann C et al (2005) A FlAsH-based FRET approach to determine G protein-coupled receptor activation in living cells. Nat Methods 2:171

Kenworthy AK et al (2004) Dynamics of putative raft-associated proteins at the cell surface. J Cell Biol 165(5):735–746

Kim SA, Schwille P (2003) Intracellular applications of fluorescence correlation spectroscopy: prospects for neuroscience. Curr Opin Neurobiol 13(5):583–590

Klonis N et al (2002) Fluorescence photobleaching analysis for the study of cellular dynamics. Eur Biophys J 31:36–51

Kohl T et al (2005) Determining protease activity in vivo by fluorescence cross-correlation analysis. Biophys J 89(4):2770–2782

Motulsky H, Christopoulos A (2004) Fitting models to biological data using linear and nonlinear regression: a practical guide to curve fitting. Oxford University Press, Oxford, chap 22, pp 138–142. Available online at http://www.graphpad.com/index.cfm?cmd=library.page&pageID=7&categoryID=1

Pando B et al (2006) Messages diffuse faster than messengers. Proc Natl Acad Sci USA 14:5338–5342

Rabut G, Ellenberg J (2004) Photobleaching techniques to study mobility and molecular dynamics of proteins in live cells: FRAP, iFRAP and FLIP. In: Goldman RD, Spector DL (eds) Live cell imaging: a laboratory manual. Cold Spring Harbor Laboratory, Cold Spring Harbor, chap 6, pp 101–127

Rich RI, Myszka DG (2000) Advances in surface plasmon resonance biosensor analysis. Curr Opin Biotech 11:54–61

Saffman PG, Delbruck M (1975) Brownian motion in biological membranes. Proc Nat Acad Sci USA 72:3111–3113

Sbalzarini I et al (2006) Simulations of (an)isotropic diffusion on curved biological surfaces. Biophys J 90:878–885

Schlessinger J et al (1976) Lateral transport on cell membranes: mobility of concanavalin A receptors on myoblasts. Proc Natl Acad Sci USA 73(7):2409–2413

Selvin PR (2000) The renaissance of fluorescence resonance energy transfer. Nat Struct Biol 7:730

Sprague BL et al (2004) Analysis of binding reactions by fluorescence recovery after photobleaching. Biophys J 86(6):3473–3495

Sprague BL, McNally JG (2005) FRAP analysis of binding: proper and fitting. Trends Cell Biol 15(2):84–91

Varma R et al (2006) T cell receptor-proximal signals are sustained in peripheral microclusters and terminated in the central supramolecular activation cluster. Immunity 25:117–127

Wu M et al (2004) Visualization of plasma membrane compartmentalization with patterned lipid bilayers. Proc Natl Acad Sci USA 101(38):13798–13803

Zal T, Gascoigne NR (2004) Using live FRET imaging to reveal early protein–protein interactions during T cell activation. Curr Opin Immunol 16:418

Zhu D-M et al (2007) Analysis of two-dimensional dissociation constant of laterally mobile cell adhesion molecules. Biophys J 92:1022–1034